DOT/FAA/TC-14/30, Rev. 1

Final Report: A Generalized Statistical Model for Aggregate Radio Frequency Interference to Airborne GPS Receivers from Ground Based Emitters

Federal Aviation Administration
William J. Hughes Technical Center
Atlantic City International Airport,
N.J. 08405

Authored by
Robert Frazier
FAA Spectrum Planning and International Group

Co-authored by
Robert Erlandson & Kenneth Peterson
National Airspace Integration Support Contract – Spectrum Engineering

August 7, 2017

Final Report

U.S. Department of Transportantion
Federal Aviation Administration

Technical Report Documentation Page

1. Report No.	2. Government Accession No.	3. Recipient's Catalog No.
DOT/FAA/TC-14/30, REV. 1		

4. Title and Subtitle	5. Report Date
Final Report: A Generalized Statistical Model For Aggregate Radio Frequency Interference To Airborne GPS Receivers From Ground Based Emitters	8/7/2017
	6. Performing Organization Code AJW-1C3

7. Author(s)	8. Performing Organization Report No.
Robert Frazier Robert Erlandson Kenneth Peterson	

9. Performing Organization Name and Address	10. Work Unit No. (TRAIS)
National Airspace Integration Support Contract (NISC) 400 Virginia Ave Suite 400 Washington DC 20024	
	11. Contract or Grant No. DTFAWA-11-C-00003

12. Sponsoring Agency Name and Address	13. Type of Report and Period Covered
Federal Aviation Administration (FAA) Spectrum Engineering Services Group (AJW-1C) 800 Independence Ave 7E-340 Washington DC 20591	
	14. Sponsoring Agency Code AJW-1C

15. Supplementary Notes

16. Abstract

A generalized analytic statistical model is presented for aggregate ground-based continuous radio frequency interference (RFI) to airborne Global Positioning Systems receivers employed in the US Air Traffic System. The model enables computation of total continuous received RFI from a random number of uniformly distributed ground-based emitters utilizing statistical path loss models to account for the propagation environment in the vicinity of metropolitan airports. Numerical results are computed for the mean and standard deviation of the aggregate received RFI power spectral density and the associated probability distribution function at the GPS L1 center frequency (1575.42 MHz) that originate from the ground-based emitters unwanted emissions. Comparisons are made between results from the generalized model and prior RFI analyses.

17. Key Words	18. Distribution Statement
Global Positioning System, GPS radio frequency interference, aggregate continuous RFI, characteristic function, propagation path loss, probability distribution function, analytic statistical interference model	

19. Security Classif. (of this report)	20. Security Classif. (of this page)	21. No. of Pages	22. Price
Unclassified	Unclassified	21	

Errata

Change Sheet for First Revision to DOT/FAA/TC-14/30 (Changes incorporated into Rev. 1):

Original version, page 6, Section 2.4.1, second paragraph:

To clarify the discussion, replaced " In our model we assume that power to be $2P_oW$ watts; i.e., an r.m.s. power spectral density of P_0 watts/Hz." with "In our model we assume that power to be $2P_oW$ Watts where W is the receiver base-bandwidth and P_o is the r.m.s. power spectral density in Watts/Hz."

Original version, page 7, Section 2.4.2, second paragraph:

To correct an error, replaced the original unnumbered equation for the parameter $\mu(r)$ with "$\mu(r) = \ln[P_o \cdot G_A(r) / PL(r)]$".

Original version, page 9, Section 3.2, seventh line:

To correct a typographic error, replaced the log-normal second moment expression "$Exp(2\mu(r)+2\sigma^2(r))$" with "$exp(2\mu(r)+2\sigma^2(r))$".

Original version, page 9, Section 3.3, second paragraph:

To correct an error similar to that in Section 2.4.2, in the definition for Γ(r), replaced the original equation with $\Gamma(r) = \exp[u'(r)] = (P_o / \overline{P_I})G_A(r) / PL(r)$".

Original version, page 11, Section 4.1.1.1:

To correct an error, replaced formula in equation (12) by $PL_{2Ray}(r) = \left(\frac{4\pi}{\lambda_c} \frac{R_{DIR}(r)}{|P_v(r)|} \right)^2$.

U. S. DEPARTMENT OF TRANSPORTATION

FEDERAL AVIATION ADMINISTRATION

FINAL REPORT: A GENERALIZED STATISTICAL MODEL FOR AGGREGATE RADIO FREQUENCY INTERFERENCE TO AIRBORNE GPS RECEIVERS FROM GROUND-BASED EMITTERS

DOT/FAA/TC-14/30, Rev. 1

AUGUST 7, 2017

This Page intentionally left blank.

Table of Contents

1 Introduction and Background

The next generation U.S. Air Traffic System (ATS), referred to as NextGen, as well as other civil airspace systems around the world are in development. Although some of the current land-based radio and radar air traffic components may operate far into the future, the new U.S. NextGen and other civil airspace system architectures will increasingly rely on satellite-based signals (e.g., the U.S. Global Positioning System (GPS)) for aircraft navigation and surveillance. GPS receivers will continue to be installed on all types of aircraft from light general aviation aircraft to commercial transports as well as military and unmanned aircraft. Dependence on GPS requires that GPS system elements meet civil aviation minimum performance standards for accuracy, availability, continuity, and integrity under stringent operating conditions. Those conditions include weak GPS signals present simultaneously with relatively strong continuous[1] radio frequency interference (RFI). One significant component of that RFI comes from non-aeronautical, ground-based sources.

The aggregate[2] RFI effect on airborne GPS receivers from this source category had been documented in several reports over the past few years ([1]-[4]). For the initial report [1], the aggregate mean received RFI was computed by two similar methods; both of which used deterministic r^{-2} path loss models. One method used a Monte-Carlo approach that generated discrete sets of random, uniformly-distributed source positions to determine both RFI mean and standard deviation. The other computed essentially the aggregate mean RFI by integration over a continuum of differential sources. A later report [2] described an analytic statistical method that introduced a probabilistic, radially-dependent individual source path loss model to account for scattering, shadowing and other propagation effects. Uniformly distributed random discrete positions were assumed for a random number of active sources (Poisson-distributed) that have a specific average surface concentration. Aggregate RFI mean and standard deviation are computed by integrating analytic functions. A cumulative probability distribution function is computed by taking the inverse Fourier transform of a related characteristic function.

Application of the analytic statistical model to a related ground-based RFI problem ([3], [4]) highlighted some weaknesses in that model. It did not account very well for the presence at shorter ranges of a strong line-of-sight RFI component and assumed a high, range-independent, single source path standard deviation. It also did not well represent the fading effect on relatively wideband RFI which would undergo frequency-selective fast fading.

To address these weaknesses a generalization of the analytic statistical model in [2] has been developed. The goal is to better quantify the effect of aggregate continuous RFI from ground-based sources to an operational aircraft GPS receiver. As in the previous work the RFI effect is determined at key waypoints along a precision approach to an airport runway. The single-path propagation model is modified to have Rician statistics and to have a range-dependent standard deviation. Utilizing these improved probability models, the mean received power spectral density, its standard deviation, and the cumulative probability distribution function associated with the aggregate received power density are each determined.

---

[1] "continuous RFI" refers to RFI that has an essentially constant mean power for a minimum time duration related to a basic receiver time constant

[2] "aggregate" refers here to the combined received power within the receiver passband from all the ground-based emitters within view of the airborne GPS receive antenna.

2 Basic Aggregate GPS RFI Analysis Method and Model Refinement Overview

The basic RFI analysis framework for this report comes from the classic "source-path-receiver" methodology as used in past RTCA and other studies (e.g., [1]-[4]). That methodology prescribes determining certain key RFI source parameters such as radiated emission power (fundamental and unwanted or unintentional), modulation type and spectral shape, carrier frequency, and antenna gain pattern. To address the aggregate RFI aspect, information is needed on the number of sources and surface concentration (sources/unit area). Key "path" characteristics include distance and direction from the receiver to the sources (largely driven by the operational scenario), propagation type (free-space or other type), and propagation statistics (as needed). The key "receiver" parameters for this report are the in-band RFI susceptibility limit (within 1575.42± 12 MHz) and the receive antenna gain pattern.

2.1 RFI Source Model

Two RFI source parameters were used in [2] to characterize the "Non-aeronautical, Off-board (ground)" sources and will be carried forward into the statistical analysis. The first source parameter, P_0, is the effective isotropic radiated power spectral density (broadband) in the GPS receive band. The selected value in logarithmic terms, -81.1 dB(W/MHz), is below the general FCC Part 15 permitted limit of -71.25 dB(W/MHz) for frequencies above 960 MHz[3]. However, it is a representative value chosen from a large collection of radiated emission test results for several common mobile and portable device types measured by NASA Langley Research Center (see discussion in section 13 of [1]).

The second RFI source parameter, ρ_E, is the active emitter surface concentration. The selected value, 10^{-4} m^{-2}, was considered in [2] to be a representative estimate. A further rationale is that busy-hour cellphone traffic estimates in metropolitan areas such as Los Angeles show about 0.78 active emitters per every 10^4 square meters without including any other sources. With Wi-Fi and other sources included, 1 emitter per 10^4 square meters is deemed for this report to be a realistic estimate for areas surrounding large metropolitan airports.

2.2 Aircraft Operational Scenario Geometry

As in previous interference studies ([1]-[3]), RFI was analyzed for three operational scenarios. Similarly, the analysis cases in this report represent the situation at three significant waypoints along a precision approach. The Final Approach Fix (FAF) waypoint is the point at which a final approach is started. The Category I Decision Height (Cat. I DH) waypoint represents the last point on the approach at which the pilot must decide that the runway visual range minimums are satisfied and the low visibility approach can be completed with visual guidance. If not, a missed approach maneuver is conducted. Similarly, the Category II Decision Height (Cat. II DH) waypoint represents the equivalent point on a Cat. II approach. Nominal aircraft heights above the runway touchdown (HAT) for those waypoints are 548 m (1799 ft.) for FAF WP, 60.96 m (200 ft.) for Cat. I DH, and 30.48 m (100 ft.) for Cat. II DH. Corresponding ground distances from the runway touchdown along the extended runway centerline for the three waypoint cases are 10463 m, 1163 m, and 581.6 m, respectively.

The nominal aircraft HAT values (referred to the aircraft "control point") need to be adjusted

[3] 47 C.F.R. 15.209 (Part B digital devices)

upward for the antenna-to-control point distance and downward for the appropriate total aircraft system error (TSE, combination of flight technical and navigation system errors). The TSE quantifies the amount that the aircraft and thus the GPS antenna is actually below the intended nominal approach path with a particular probability. With the same assumptions for those corrections as used in [2], the resulting GPS receive antenna HAT for the three RFI analysis cases are shown in table 1.

Table 1 Operational Scenario Case Aircraft-Related Heights

Operational Scenario Case	Nominal Aircraft HAT (m)	Antenna Offset (m)	TSE Offset (m)	Corrected Antenna HAT (m)
FAF WP	548.33	+2.13	-15.24	535.2
Cat. I DH	60.96	+2.13	-9.75	53.34
Cat. II DH	30.48	+2.13	-6.67	25.94

Figure 1 illustrates a side profile view of the precision approach geometry (e.g., for the case of FAF WP, H_{AF} = 548.33 m, TSE_F = 15.24 m, and antenna offset = 2.13 m). Figure 2 shows the general approach case geometry top view that contains an RFI source exclusion zone.

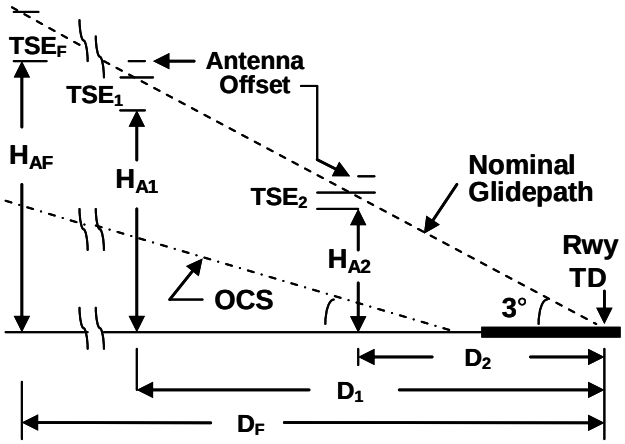

Figure 1 Runway Precision Approach Geometry - Vertical Profile View

Geometric factors are shown for GPS antenna height (H_A) derivation in Category I and II precision approach and Final Approach Fix cases on a 3° glidepath approach. The term "OCS" refers to the obstacle clearance surface for the precision approach.

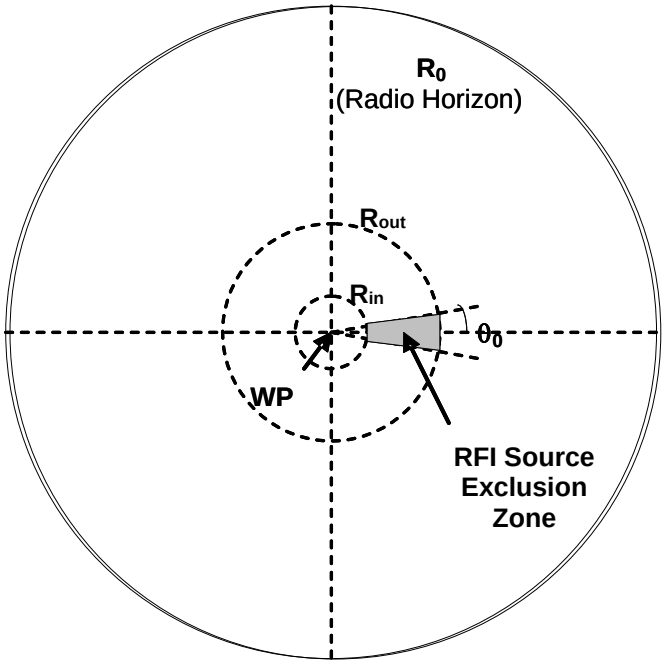

Figure 2 Runway Approach Geometry - Top View
Geometric factors are shown for RFI source exclusion zone and radio horizon (outer limit of RFI source radius). The central point (WP) refers to the ground track point directly under the aircraft for each approach waypoint case.

For the FAF waypoint case, RFI sources are assumed to be distributed over the whole ground area out to the radio horizon (area inside the circle of radius R_0). However, a modification is made for the two lower height cases where the aircraft is considerably closer to the airport runway. For those cases we will assume, similar to [2], that RFI sources are excluded from an annular sector representing the airport runway obstacle clearance zone. The Category I DH case exclusion zone annular sector extends from 488 to 5830 meters from the ground track nadir point with a half-angular width of 17 degrees. Similarly, the equivalent parameters for the Category II DH case are 44.9 m, 2842 m, and 25 degrees.

2.3 Airborne GPS Receive Antenna Gain Model

In a computation of aggregate RFI power from ground-based sources for an airborne GPS receiving system, RFI signals must be assumed to be arriving from essentially all directions below the horizon. As such RTCA SC-159 worked to develop over some time a representative lower hemisphere antenna gain pattern model for the GPS receive antenna mounted on the top of the aircraft fuselage [1]. The pattern model is assumed to be azimuthally symmetric and dependent only on elevation angle from the aircraft horizon and represents the maximum gain for any RFI signal polarization. The gain pattern model is dependent somewhat on the approach category for which the aircraft is certified.

The lower hemisphere aircraft antenna pattern model in terms of gain versus elevation angle (angle between the aircraft horizon and the line joining aircraft and RFI source) is illustrated in figure 3.

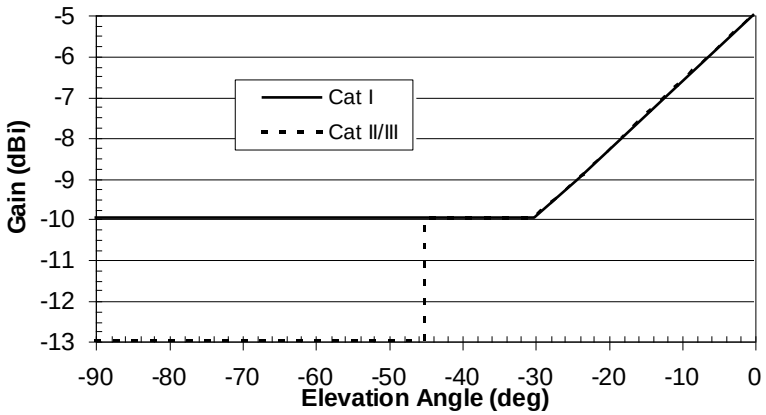

Figure 3 Lower Hemisphere Installed Antenna Pattern Max. Gain vs. Elevation Angle
The solid line is for aircraft equipped for non-precision or Category I precision approach operation. The dashed line is for aircraft equipped for a Category II or III precision approach.

For aircraft performing non-precision or Category I precision approaches, the receive lower hemisphere elevation antenna gain is given by:

$$G_A(r) = \begin{bmatrix} 10^{-1}, & 0 \le r \le \sqrt{3}\left(H_A - H_E\right) \\ -1+\left(0.5-\frac{3}{\pi}\tan^{-1}\left(\frac{H_A-H_E}{r}\right)\right) & \\ 10 & , \ \sqrt{3}\left(H_A - H_E\right) \le r \end{bmatrix} \quad (1)$$

where G_A is the antenna power gain (algebraic ratio) and H_A, H_E, and r are, respectively, the aircraft and RFI source antenna heights and the radial separation distance from the aircraft ground track nadir point to the base of the RFI source antenna (all in meters). Note in the gain formulas that the term $\tan^{-1}((H_A-H_E)/r)$ is the magnitude of the elevation angle in radians from the GPS antenna to the RFI source with $H_A > H_E$. For an aircraft equipped for Category II or III precision approach, the corresponding receive antenna gain is given by:

$$G_A(r) = \begin{bmatrix} & \\ 10^{-1.3}, & 0 \le r \le \left(H_A - H_E\right) \\ 10^{-1}, & \left(H_A - H_E\right) \le r \le \sqrt{3}\left(H_A - H_E\right) \\ -1+\left(0.5-\frac{3}{\pi}\tan^{-1}\left(\frac{\left(H_A-H_E\right)}{r}\right)\right) & \\ 10 & , \ \sqrt{3}\left(H_A - H_E\right) \le r \end{bmatrix} \quad (2)$$

2.4 Probabilistic Path Loss Model Refinement

As was shown in [2], in order to determine statistical information regarding aggregate interference power, it is first necessary to model the statistics of interference from a single emitter as impacted by the propagation environment. One significant modification allows the new model to account for the possibility of a strong line-of-sight interfering signal which may be range and height dependent. That modification replaces the underlying probabilistic path loss

model in which the received interference signal envelope is described by a hybrid Rayleigh-lognormal distribution (Suzuki distribution) with one having a hybrid Rician-lognormal distribution (extended Suzuki distribution [9]). The Rician portion of the distribution allows for a line-of-sight component which may vanish with increased range, thus changing to a Rayleigh distribution at longer ranges where all of the scattering is expected to be diffuse. As discussed in section 2.4.1 below, wideband interference is represented in the new model by the addition of several random variables each of whose envelope is probabilistically described by the extended Suzuki distribution.

An additional shortcoming of the previous model was that the standard deviation associated with the log-normal component of the hybrid distribution was a constant independent of radial separation. It was noted in [4] that when a strong line-of-sight interfering signal is present, the standard deviation of the lognormal component must be very small compared to the case when all of the scattering is diffuse. This deficiency is corrected in the new model by incorporating a range dependent standard deviation for the lognormal component.

2.4.1 Revised Fading Model

The propagation channel is typically modeled as a product of a slow fading process (log-normal power distribution) and a fast fading process [8]. The fast fading portion may be either "flat" (maximum delay spread, $\tau_{ds} << 1/W$; where W=interference signal base-bandwidth) or it may be frequency selective. The simplest case to model is the case where the fast fading is flat. In that case, the received interference from a single emitter, $\gamma(t)$, may be written as $\gamma(t) = \mathrm{Re}\{\alpha(t)\beta(t)s_E(t)\}$ where Re{ } denotes the real part, while α, β, and s_E are independent complex random processes. The term $\alpha(t)$ denotes the fast fading process, $\beta(t)$ the slow fading component, and $s_E(t)$ the portion of the interfering emitter signal falling into the GPS L1 band with center frequency f_c ($s_E(t) = u(t)\exp(i2\pi f_c t)$ where u(t) is complex).

In the generalized model, α has independent normally distributed real and imaginary parts each with mean values that may be different from zero to account for the presence of a strong line-of-sight component at shorter ranges. Thus, $|\alpha(t)|^2$, has a non-central Chi-squared distribution with two degrees of freedom. Although $|s_E(t)|^2$ is a random process, to avoid dealing with those statistics the instantaneous power associated with the single source emission (unwanted emission in this situation) is deemed to be constant as in most of the literature on path loss models. In our model we assume that power to be $2P_oW$ Watts; where W is the receiver base-bandwidth and P_0 is the r.m.s. power spectral density in Watts/Hz. Under these assumptions, the random process $|\beta(t)s_E(t)|^2$ is log-normally distributed and the received single emitter interference power $|\gamma(t)|^2$ becomes the product of two random variables, one having a non-central Chi-squared distribution while the other is log-normally distributed.

For a scenario with frequency selective fast fading, it can be shown [10] that γ can be approximated as the sum of several independent flat fading processes. Thus, $\gamma(t)$ is written as $\gamma(t) = (\sum_{l=0}^{L-1} \alpha_l(t)s_E(t-\tau_l))\beta(t)$; where the channel parameter, L, is the number of resolvable fast

fading paths and the τ_l are chosen such that $E[s_E(t-\tau_i)s_E(t-\tau_k)]=0$ for $k \neq l$. Then the instantaneous power, $|\gamma(t)|^2$, becomes $|\gamma(t)|^2 = (\sum_{l=0}^{L-1} |\alpha_l(t)|^2 |s_E(t-\tau_l)|^2) |\beta(t)|^2$.

Using the same assumption as above regarding the single emitter power, the received single emitter power density may be written as:

$$|\gamma(t)|^2_{density} = \underbrace{(\sum_{l=0}^{L-1} |\alpha_l(t)|^2)}_{FastFading} \overbrace{|\beta(t)|^2 P_o}^{SlowFading}.$$

This form for the received single emitter power density is the most flexible and is the form adopted in the new generalized model. The slow fading portion is log-normally distributed with parameters μ and σ while the fast fading process has a non-central Chi-squared distribution with 2L degrees of freedom and parameters ρ_o and ψ_o (more on these parameters in section 2.4.2).

In the generalized model each of these parameters are range dependent hence we may express the received single emitter power spectral density as

$$P_E(r) = \Sigma(r)\Omega(r),$$

where Σ denotes the fast fading component and Ω the slow fading. Note all time dependence has been dropped as all of the constituent processes are assumed to be stationary.

2.4.2 Median Path Loss and Fading Model Parameters Overview

The propagation environment is modeled probabilistically with a range and height-dependent median path loss to an individual RFI source. Based on a flat-Earth assumption, a continuous median path loss function (*PL(r)*) is generated by combining 3 range segment models taken in part from mobile radiotelephone propagation studies. The long range segment model (*r* typically greater than 1 km) is based on the Hata-Okumura model [5]-[6] (suburban case). Two options are used for the mid-range segment model (depending on aircraft antenna height): Erceg/Greenstein [7] ($H_A \leq 80$ m), or a log-log constant slope blend ($H_A > 80$ m). The short range segment model (ranges less than a few hundred meters) is the classic Two-Ray [8] with concrete as the single reflecting surface. Reciprocity is assumed to hold as it relates to the probabilistic modeling of the propagation channel. Details for actual segment breakpoint ranges which depend on the difference between receiver and source antenna heights (H_A-H_E) are given in section 4.

With the median path loss function, *PL(r)*, defined for any individual source, the single-path median received power parameter, $\mu(r)$, can be written as $\mu(r) = \ln[P_o \cdot G_A(r) / PL(r)]$; where P_0 is the RFI source isotropic emission power spectra density (see section 2.1) and $G_A(r)$ is the airborne GPS receive antenna gain (see section 2.3). The single-path range-dependent standard deviation associated with the median received power is σ(r) (see section 4.1.2). Three parameters are needed to represent the fast fading statistics. The range-independent channel parameter, *L*, mentioned in section 2.4.1, is defined numerically as $L = \lceil \tau_{DS} W \rceil$; where the operator $\lceil \ \rceil$ implies rounding up the operand to the next integer, τ_{DS}, is the spread in channel delay time, and *W* is the channel baseband bandwidth. The other two parameters, $\rho_0(r)$ and $\psi_0(r)$, are multiplicative factors that specify, respectively, the proportion of direct line-of-sight

propagation and diffuse scattering present on a particular path (section 4.1.2 has more specific details).

3 Derivation of Refined RFI Statistical Model

3.1 Mean Aggregate Power Density

The aggregate received power spectral density P_I at the aircraft GPS antenna can be written as

$$P_I = \sum_{k=0}^{n} P_{E_k}(r_k) \tag{3}$$

where $P_E(r)$ is as defined in section 2.4.1 and r_k is the radial distance to the kth emitter.

The mean aggregate power $\overline{P_I}$ is obtained following the methodology[4] given in [2] as

$$\overline{P_I} = E[P_I] = E[n]E[P_E] = \bar{n}E[\Sigma(r)]E[\Omega(r)],$$

or in terms of parameters described in Sec. 2.4.2,

$$\overline{P_I} = \bar{n}\int_0^{R_o} (2L\psi_o(r) + \rho_o^2(r)) \exp[\sigma^2(r)/2 + \mu(r)] f(r) dr . \tag{4}$$

In Equation (4), $\bar{n}$ is the mean number of active emitters (Poisson-distributed) within the radio horizon radius, R_0. The expression, $(2L\psi_o(r) + \rho_o^2(r))$, is the first moment (mean) of the non-central Chi-squared fast-fading distribution and the expression, $\exp\left[\sigma^2(r)/2 + \mu(r)\right]$, is the log-normal slow-fading distribution mean.

For an aircraft operational scenario with no emitter exclusion zone, the source location radius probability function, *f(r)*, in Equation (4) is given as

$$f(r) = 2r / R_o^2, \ 0 \le r \le R_o, \tag{5}$$

where $R_0 = 1000(\sqrt{17.008H_A} + \sqrt{17.008H_E})$ meters.

In a scenario that includes an annular segment exclusion zone as shown in figure 2,

$$f(r) = \begin{Bmatrix} 2\pi r / (\pi R_o^2 - \theta_o(R_{out}^2 - R_{in}^2)), & 0 \le r < R_{in} \\ 2(\pi - \theta_o) r / (\pi R_o^2 - \theta_o(R_{out}^2 - R_{in}^2)), & R_{in} \le r < R_{out} \\ 2\pi r / (\pi R_o^2 - \theta_o(R_{out}^2 - R_{in}^2)), & R_{out} \le r \le R_o \end{Bmatrix}, \tag{6}$$

where θ_0 is the exclusion zone annulus half-angle and R_{in} and R_{out} are respectively, the inner and outer annular radii [2]. Note for the case with no exclusion zone, the mean number of active emitters $\bar{n} = \pi\rho_E R_o^2$ while $\bar{n} = \rho_E(\pi R_o^2 - \theta_o(R_{out}^2 - R_{in}^2))$ when an exclusion zone is present.

[4] Note that *E[ ]* is the Expected Value operator

3.2 Aggregate Standard Deviation

As in [2], the standard deviation is determined for the normalized random variable $P_I / \overline{P_I}$ rather than P_I for ease of numerical computation. Then following the methodology in [2] we obtain

$$\sigma_I = \sqrt{\bar{n} E[(P_E(r))^2]} / \overline{P_I} \,. \tag{7}$$

However, $E(P_E^2(r)) = E[E(P_E^2(r) \mid r)]$ where $E(P_E^2(r) \mid r)$ is the product of the second moment of the Chi-squared distribution and the second moment of a log-normally distributed random variable. The second moment of the Chi-squared distribution can be shown to be given by $(L\psi_o(r) + \rho_o^2(r))^2 + 2(L\psi_o^2(r) + 2\psi_o(r)\rho_o^2(r))$. The second moment of the log-normal distribution is $exp(2\mu(r) + 2\sigma^2(r))$. Hence

$$\sigma_I = \sqrt{n \int_0^{R_O} (L\psi_O(r) + \rho_O^2(r))^2 + 2(L\psi_O^2(r) + 2\psi_O(r)\rho_O^2(r)) exp[2\mu(r) + 2\sigma^2(r)] f(r) dr} / \overline{P_I} \,. \tag{8}$$

3.3 Aggregate Cumulative Probability Distribution Function Derivation

The cumulative probability distribution is determined by first computing the characteristic function, $C(\tau)$. To determine the characteristic function associated with the received interference power, P_I, we begin by normalizing the random variable using its mean. Thus we find the characteristic function for the new random variable $P_I / \overline{P_I}$ as this will be more tractable from a numerical computation perspective. In [2] it was shown that this characteristic function can be expressed as

$$C(\tau) = \exp[-\bar{n}(1 - \phi(\tau))] \tag{9}$$

where $\phi(\tau) = E[\exp(i\tau P_E(r) / \overline{P_I})]$, i.e., $\phi(\tau)$ is the characteristic function of the interference from a single emitter normalized by the mean aggregate interference power.

Then, $\phi(\tau) = E[\exp(i\tau P_E(r) / \overline{P_I})] = E[\exp(i\tau \Sigma(r) \Omega'(r))]$; where $\Omega'(r) = \Omega(r) / \overline{P_I}$.

Now $E[\exp(i\tau \Sigma(r) \Omega'(r))] = E[E[\exp(i\tau \Sigma(r) \Omega'(r)) \mid \Omega', r]]$. Since the characteristic function of the Non-central Chi-squared distribution is known, we have,

$E[\exp(i\tau \Sigma(r) \Omega'(r)) \mid \Omega', r] = \exp[i\tau \Omega'(r) \rho_o^2(r) / (1 - 2i\psi_o(r) \Omega'(r) \tau)] / (1 - 2i\psi_o(r) \Omega'(r) \tau)^L$.

We also write, $E[\exp(i\tau \Sigma(r) \Omega'(r))] = E[E[\exp(i\tau \Sigma(r) \Omega'(r)) \mid r]]$.

But, $E[\exp(i\tau \Sigma(r) \Omega'(r)) \mid r] = E[\int_{\Omega'} E[\exp(i\tau \Sigma(r) \Omega'(r)) \mid \Omega', r] p_{\Omega'}(\Omega') d\Omega']$;

where $p_{\Omega'}(u) = (1 / (u\sqrt{2\pi}\sigma(r))) \exp[-(\ln(u) - \mu'(r))^2 / (2\sigma^2(r))]$.

If we let $\Gamma(r) = \exp[u'(r)] = (P_o / \overline{P_I}) G_A(r) / PL(r)$, and make the substitution $x = \ln(u / \Gamma(r))$, we may write,

$\phi(\tau) = \int_0^{R_o} \int_{-\infty}^{\infty} S(\tau, r, x) [(1 / (\sqrt{2\pi}\sigma(r))) \exp(-x^2 / (2\sigma^2(r))) f(r) dx dr$; where

$S(\tau, x, r) = [1 / (1 - 2i\tau\psi_O(r)\Gamma(r)\exp(x))^L] \exp[i\tau\Gamma(r)\exp(x)\rho_O^2(r) / (1 - 2i\tau\psi_O(r)\Gamma(r)\exp(x))]$.

As in [11] we substitute $y = x / (\sqrt{2}\sigma(r))$ and obtain

$$\phi(\tau) = \int_{-\infty}^{\infty} \int_{0}^{R_o} (1/\sqrt{\pi}) \Phi(\tau, y, r) f(r) Exp(-y^2) dr dy \text{ ; where}$$

$$\Phi(\tau, y, r) = [1/(1 - 2i\tau\psi_O(r)\Gamma(r)\exp(\sqrt{2}\sigma(r)y))^L] \exp[i\tau\Gamma(r)\exp(\sqrt{2}\sigma(r)y)\rho_o^2(r)/(1 - 2i\tau\psi_O(r)\Gamma(r)\exp(\sqrt{2}\sigma(r)y))] .$$

Further, as in [11] we use the K-point Hermite-Gauss quadrature method with weights w_k and nodes y_k to write:

$$\phi(\tau) \approx \sum_{k=1}^{K} (w_k / \sqrt{\pi}) \int_{0}^{R_o} \Phi(\tau, y_k, r) f(r) dr . \tag{10}$$

A value of 65 has been used for K to obtain very good accuracy in (10).
Finally using (9) we obtain the cumulative distribution function for the random variable $P_I / \overline{P_I}$ as in [12],

$$\Pr(P_I / \overline{P_I} < z) = (1/(2\pi)) \lim_{A \to \infty} \int_{-A}^{A} ((1 - \exp(-i\tau z)) / (i\tau)) C(\tau) d\tau + (1/2)\exp(-\bar{n}) \tag{11}$$

for $z > 0$.

4 Detailed Computational Model Parameters and Numerical Results

Given the basic analysis framework and model elements as described in section 2 and the revised statistical formulas derived in section 3 above, the RFI analysis structure for this report has been established. The following subsections provide more details of certain necessary computational parameters (e.g., path loss segment and other breakpoint radii) together with path loss and fading functions for the 3 operational cases and then present and discuss the analysis results.

4.1 Detailed Computational Model Parameters

4.1.1 Isotropic Median Path Loss Function Details

4.1.1.1 Short-Range Median Path Loss Segment Model and Related Parameters

As noted earlier for short range paths ($r < R_1$), a Two-Ray path loss model [2] is assumed. Besides explicit dependence on radial separation range, r, the isotropic path loss depends on the direct and reflected ray path lengths and the relative transmission phase difference between the two ray paths. It also depends on the electrical parameters of the reflecting surface (here assumed to be concrete). The direct and reflected ray path lengths are defined respectively as: $R_{DIR}(r) = \sqrt{(H_A - H_E)^2 + (r)^2}$ and $R_{REFL}(r) = \sqrt{(H_A + H_E)^2 + (r)^2}$ and the reflected ray relative phase lag is $\phi(r) = \left(2\pi/\lambda_c\right)(R_{REFL}(r) - R_{DIR}(r))$, where λ_c is the free-space wavelength at the receiver center frequency, f_c, (1575.42 MHz in this report). The grazing angle, $\theta(r)$, of the reflected ray with the concrete reflecting surface is given as $\theta(r) = \sin^{-1}((H_A + H_E)/R_{REFL}(r))$. Two electrical parameters of concrete (relative dielectric constant, ε_r = 7.0, conductivity, σ_{cc} = 0.15 S/m) are used to form a constituent ratio parameter, $x = \sigma_{cc}/2\pi f_c \varepsilon_0$, where ε_0 is the free space permittivity. With the ratio parameter, x, defined, the complex reflection coefficient for vertical polarized

waves, $\rho_V(r)$, is given as $\rho_v(r) = \dfrac{(\varepsilon_r - i\cdot x)\sin(\theta(r)) - \sqrt{(\varepsilon_r - i\cdot x) - \cos^2(\theta(r))}}{(\varepsilon_r - i\cdot x)\sin(\theta(r)) + \sqrt{(\varepsilon_r - i\cdot x) - \cos^2(\theta(r))}}$ where the imaginary constant, $i = \sqrt{-1}$. The complex multi-path field factor at the receive antenna is then given by $P_v(r) = 1 + \left(R_{DIR}(r) \big/ R_{REFL}(r) \right) \rho_v(r) \cdot e^{-i\phi(r)}$. With these definitions the Two-Ray isotropic median path loss is written (algebraic terms) as $PL_{2Ray}(r) = \left(\dfrac{4\pi}{\lambda_c} \cdot \dfrac{R_{DIR}(r)}{|P_v(r)|} \right)^2$ (12)

4.1.1.2 Mid-Range Median Path Loss Segment Model and Related Parameters

Since the long range model described below is not really valid for separation ranges less than 1 kilometer and the Two-Ray model is probably unrepresentative beyond a few hundred meters (depending on the antenna height difference, H_A-H_E), a mid-range segment model is needed in between to form a continuous function overall ($R_1 < r < R_2$). One of two options is used in this report as determined by the value of H_A. As in [2] when the aircraft antenna height, $H_A \le 80$ m (CAT I and II DH), a modified[5] Erceg/Greenstein model is used. Median path loss (in algebraic terms) is

$$PL_{EG,\text{mod}}(r) = A^2 \cdot \left(\frac{r}{r_0} \right)^{a - b\cdot H_A + c/H_A} \quad (13).$$

In (13) $A = 4\pi r_0/\lambda_c$ with $r_0 = 100$ m. Values for constants a (=3.6), b (=0.005), and c (=20.0) are chosen to represent the area in the vicinity of an airport (terrain model C (flat, light tree cover)).

As in [2] for cases when $H_A > 80$ m (the FAF Waypoint in this report), a log-log, constant slope blending function is used. The function's range term constant exponent and intercept point are chosen to achieve continuity at either end with the short- and long-range path loss functions given appropriate segment breakpoints.

4.1.1.3 Long-Range Median Path Loss Segment Model and Related Parameters

Similar to the approach in [2] for separation ranges more than R_2 (> 1 km), the Hata-Okumura median propagation loss model [5], [6] is used. The area around the airport is modeled by inserting Hata's suburban constants in the equations. The median isotropic path loss (in algebraic terms) is

$$PL_{HS}(r) = 10^{\alpha + \beta_c \cdot (\log(r/1000))^{F(r,H_A)}} \quad (14);$$

where $\alpha = 0.1\left[69.12 + 26.16\cdot\log(f_c) - 2\cdot\log^2\left(f_c/28 \right) - 13.82\cdot\log(H_A) - 3.2\cdot\log^2(11.75H_E) \right]$,

$\beta_C = 0.1\cdot\left[44.9 - 6.55\cdot\log(H_A) \right]$ and $F(r, H_A) = 1$, $r \le 20$ km, or

$$F(r,H_A) = 1 + \left[0.014 + 1.87\cdot10^{-4}(f_c) + 1.87\cdot10^{-3}H_A \big/ \left(1 + 7\cdot10^{-6}H_A\right) \right] \log\left(r/2\cdot10^4\right)^{0.8}, \; r > 20\text{km}$$

[5] The modification here involves using a different range-dependent $\sigma(r)$ with the E/G median formula.

4.1.1.4 Path Loss Range Segment Breakpoint Strategy

The strategy for choosing the path loss segment breakpoints (i.e., the inner and outer radial limits R_1 and R_2 of the mid-range segment) is driven by several factors. The main one is aircraft antenna height (H_A) which directly controls the selection of the mid-range median path loss model as indicated in section 4.1.1.2. If the Erceg/Greenstein model is indicated, the next step to find R_1 is to determine the intersection of the Erceg/Greenstein with the Two-Ray path loss associated with that H_A value. Since the Two-Ray model will have slight oscillations near the intersection radius, there may be a small number of possible intersections. A limiting condition to help select one intersection value is that R_1 should be greater than about 100 m (due to an Erceg/Greenstein model constraint). The relative loss slope difference between the Erceg/Greenstein and Hata-Okumura model segments is another factor (H_A and H_E values contribute to the slope difference). With R_1 fixed, the relative slope difference and Hata-Okumura path loss intercept parameter, α, control the outer radius R_2, the intersection between the mid- and long-range segments.

When aircraft antenna heights are above 80 meters, the strategy for the mid-range segment median path loss breakpoints is somewhat different than for the lower height cases. This difference comes in part from the lack of a firm inner radius constraint for the log-log, constant-slope blending function. However, to preserve some consistency with the lower height cases, the mid-range segment inner radius, R_1, is set to give a Two-Ray segment grazing angle, $\theta(r)$ such that $\tan(\theta(R_1)) \cong 0.5$. Some slight adjustment of the R_1 value may be done, if needed, to reduce the loss slope change at the junction with the Two-Ray segment. In a similar way, the outer radius, R_2, is set to give an elevation angle from the source to the receive antenna, $\varepsilon(r)$, such that $\tan(\varepsilon(R_2)) = 1/14$ (i.e.; $\varepsilon(R_2) \cong 4°$).

4.1.2 Statistical Variable Function Details

As discussed in section 2.4., use of three single-path range-dependent statistical variable parameters, $\sigma(r)$, $\rho_0(r)$, and $\psi_0(r)$ is proposed to refine and generalize the analytic statistical model from [2]. In general, the range dependence of these parameters should be associated with the path loss segment behavior. For example, the standard deviation $\sigma(r)$ should be low at very short ranges where there is simple 2-ray propagation and gradually rise to a maximum value at a radius where there is significant scattering (i.e.; the boundary between the short- and mid-range path loss segments). Similar behavior should be expected for the diffuse scattering factor $\psi_0(r)$, but the line-of-sight factor, $\rho_0(r)$, should behave in the opposite manner (high at very short ranges and zero when scattering dominates).

For this report a linear transition region is proposed between the very short range condition and the onset of significant scattering (chosen to be the mid-range segment inner radius). The transition region starting point is chosen as the radius, r_s, such that the elevation angle from the source to the receive antenna, $\varepsilon(r_s) = 45°$ (i.e.; $r_s = H_A - H_E$). The transition end point is the radius R_1 previously defined in section 4.1.1.4. For convenience, the single-path standard deviation, $\sigma(r)$, is described in decibel terms. Similar to the strategy used in [4], the short-range and full-scattering $\sigma(r)$ limits in this report are 0.5 dB and 6.4 dB, respectively. In this report, however, a

log-linear function in range is used. Thus $\sigma_{dB}(r) = \begin{Bmatrix} 0.5, & 0 \le r \le r_s \\ 0.5 + 5.9\dfrac{(r - r_s)}{(R_1 - r_s)}, & r_s < r \le R_1 \\ 6.4, & r > R_1 \end{Bmatrix}$ (15)

In a similar form the unitless line-of-sight parameter, $\rho_0(r)$, is specified as its square as

$$\rho_0^2(r) = \begin{Bmatrix} 1.0, & 0 \le r \le r_s \\ 1.0 - \dfrac{(r - r_s)}{(R_1 - r_s)}, & r_s < r \le R_1 \\ 0, & r > R_1 \end{Bmatrix} \quad (16)$$

Again for convenience, the unitless diffuse scattering parameter, $\psi_0(r)$, is specified in terms of a product with channel parameter, L, as

$$2L\psi_0(r) = \begin{Bmatrix} 0.1, & 0 \le r \le r_s \\ 0.1 + 0.9\dfrac{(r - r_s)}{(R_1 - r_s)}, & r_s < r \le R_1 \\ 1.0, & r > R_1 \end{Bmatrix} \quad (17)$$

Note in (17) that the composite parameter $2L\psi_0(r)$ is non-zero at short ranges ($< r_s$). This aspect is justified for consistency with the assumption that $\sigma(r)$ is also non-zero over the same ranges. This is to associate the small $\sigma(r)$ value with a small amount of diffuse scattering in the propagation loss at short ranges. For this report $L = [\tau_{DS} \cdot W] = [0.5\mu s \text{ x } 2.0 \text{ MHz}] = 1$.

4.2 Mean Aggregate Power Density and Standard Deviation and Related Results

4.2.1 Summary of Median Path Loss Parameters and Other Related RFI Parameters

With the computational parameter and statistical variable definitions from section 4.1, the blended median isotropic path loss function can be determined for each of the three operational cases. Table 2 summarizes key path loss and related mean received power parameters.

Table 2 Key Parameters for the Median Path Loss and Median Received Power Functions

`	FAF WP Case	Cat. I DH Case	Cat. II DH Case
Receive Antenna. Ht. (m)	535.2	53.34	25.94
Std. Dev. Inner Radius, r_s (m)	533.4	51.54	24.14
Mid-range Inner Rad. R_1 (m)	1054.237	111.149	99.3811
Mid-range Outer Rad. R_2 (m)	7502.3	11227.6	2475.381
Mid-range Log-Log slope	3.3194	N/A	N/A
Mid-range E/G loss slope	N/A	3.708	4.241
Long-range Hatta loss slope	2.7028	3.3578	3.5638
Excl. Zone Half-angle (deg)	0.0	17	25
Excl. Zone Inner Rad. (m)	N/A	488.0	44.93
Excl. Zone Outer Rad. (m)	N/A	5830.0	2842
Radio Horizon Radius (km)	100.941	35.653	26.537

As discussed in section 2, common source-related constants assumed for all analysis cases are the EIRP density (P_0) of -81.1 dB(W/Hz), surface concentration (ρ_E) of 10^{-4} m^{-2}, and antenna height (H_E) of 1.8 m.

4.2.2 Median Isotropic Path Loss and Statistical Variable Function Results

The blended 3-segment median isotropic path loss plots for the FAF WP (figure 4) and Cat. II DH (figure 5) analysis cases illustrate the primary radial-dependent component in the median single-path received RFI parameter, $\mu(r)$, in those cases. Note how the magnitude of the path loss is higher in the FAF case versus the Cat. II case at short ranges but at ranges beyond 350 meters the Cat. II case loss magnitude is higher.

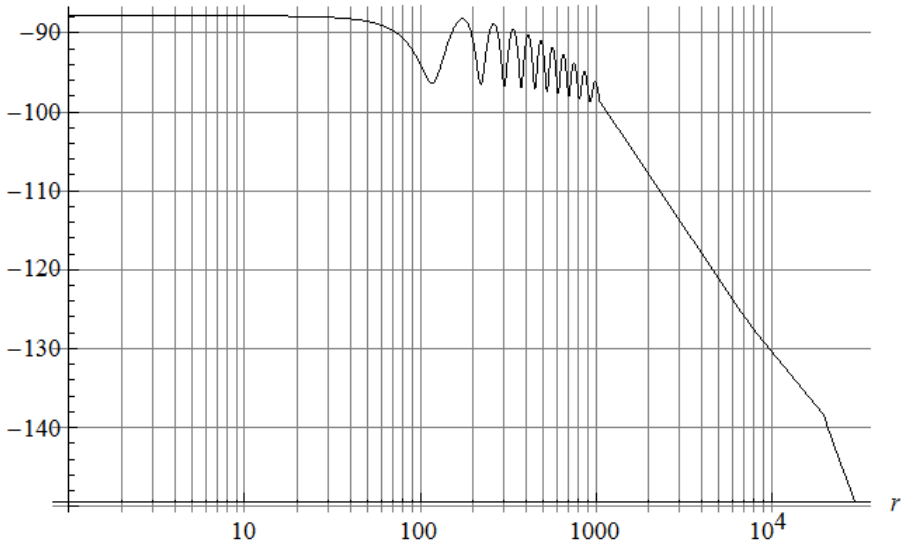

Figure 4 FAF PL (-dB) vs Radial Separation Range (m)

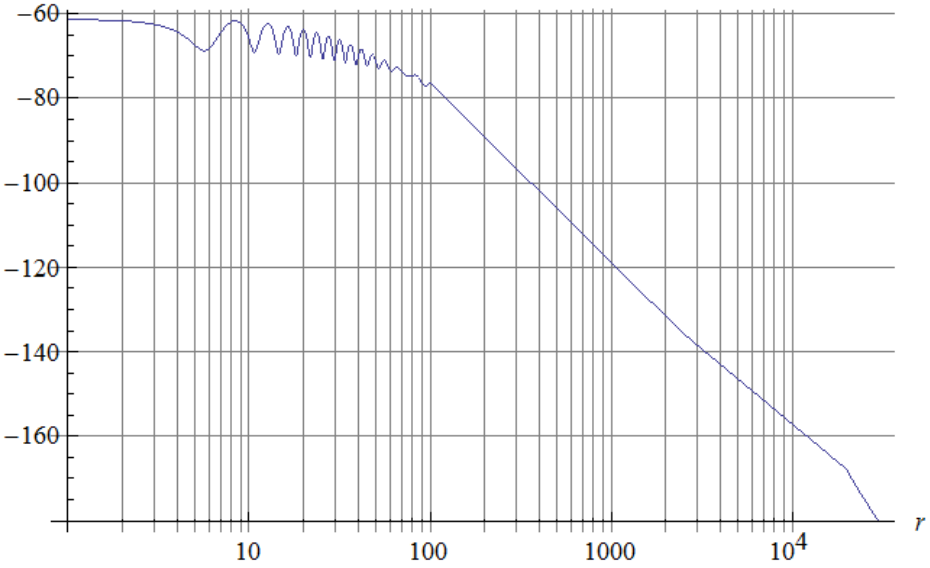

Figure 5 Cat. II DH PL(-dB) vs Radial Separation Range (m)

Examples of the statistical variable function, $\sigma_{dB}(r)$, along with the Non-central Chi-squared first and second moment functions, *FB(r)*, and *m2Xsq(r)*, respectively, (which are functions of the basic statistical parameters, $\rho_0(r)$, $\psi_0(r)$, and L) are shown for the Cat. I DH case (figure 6).

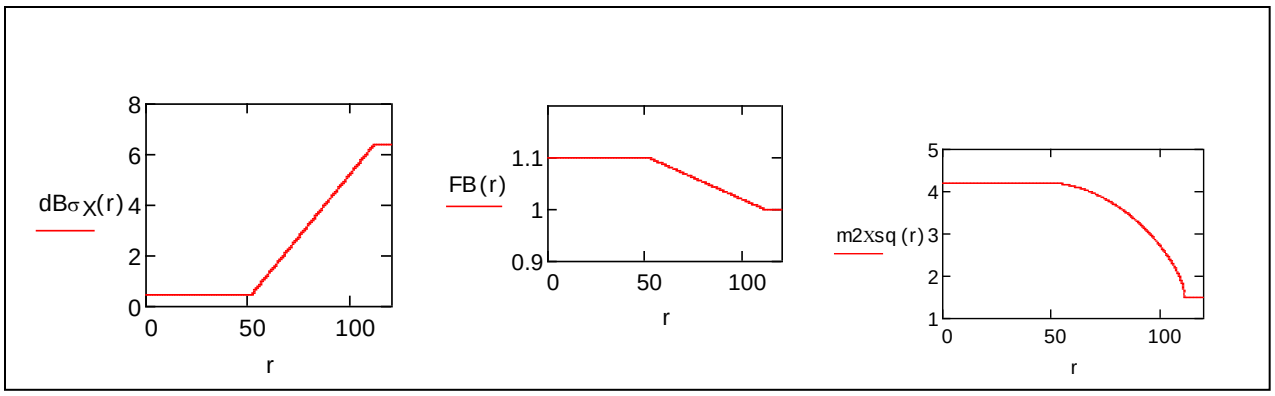

Figure 6 Statistical Variable Functions vs. Radial Separation Range for the Cat. I DH Case
(Limits for 1st moment function labeled $FB(r) = 2L\psi_0(r)+\rho_0^2(r)$, are 1.1 and 1.0)
(Limits for 2nd moment function, labeled *m2Xsq(r)*, are 4.205 and 1.5)

4.2.3 Mean Aggregate Received Power Density and Standard Deviation Results

The median path loss and statistical variable functions together with the parameters described above were inserted appropriately into Equation (4) to compute the mean aggregate received power density for the three operational scenario cases. With those mean values, the normalized aggregate power density random variable was formulated and its standard deviation computed with Equation (8) for the same three cases. Table 3 lists those results and together with comparable ones from the initial study [2].

Table 3 Operational Case Mean Aggregate Received Power Density and Standard Deviation

Operational Scenario Case	Initial Model Aggregate Mean (dBW/MHz)	Initial Model Standard Deviation (ratio)	New Model Aggregate Mean (dBW/MHz)	New Model Standard Deviation (ratio)
FAF WP	-151.17	0.2303	-153.609	0.06345
Cat. I DH	-151.11	2.37335	-153.673	0.6998
Cat. II DH	-149.86	3.1625	-152.667	1.0337

Compared to the new generalized model, the initial model mean and standard deviation were larger due in part to the large, range-independent, single-path standard deviation value 8.34 dB that was assumed. The change from Rayleigh to Rician fast fading with Non-central Chi-squared probability distribution also helped reduce the new results. Overall reductions are 2.4 to 2.8 dB on the mean and 3.1 to 3.6x on standard deviation. The new model results are believed to be more representative of the actual environment, but that assessment needs further verification.

4.3 Characteristic Functions and Cumulative Probability Distribution Function Results

4.3.1 Characteristic Functions for Cumulative Probability Distribution Calculations

The probability distribution function given in (11) is uniquely determined by its characteristic function. This characteristic function is in turn dependent on the particular path loss model associated with a given operational scenario case. Thus there is a different probability distribution for each of the operation scenario cases. To evaluate the probability distribution function associated with a particular case, its characteristic function must first be determined. These characteristic functions have been computed as per (9) and (10). Figures 7 and 8 show the characteristic function for the FAF waypoint and Category II decision height cases, respectively.

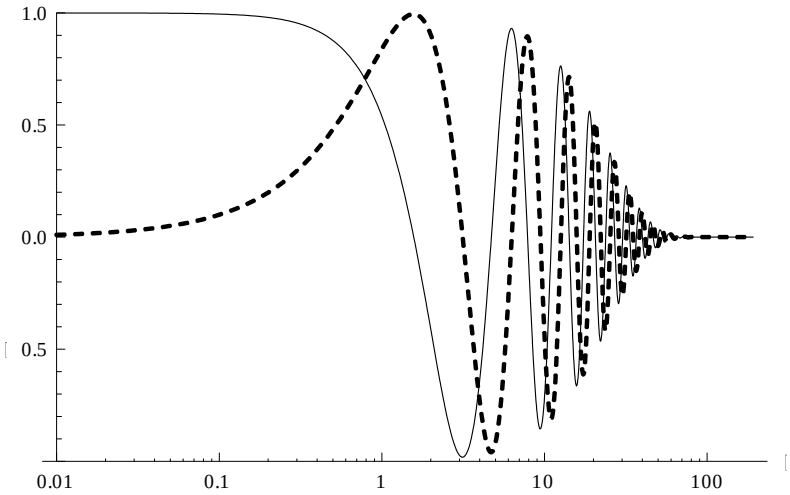

Figure 7 Complex Characteristic Function C(τ) versus τ for the FAF WP case
(real part=solid line, imaginary part=dashed line)

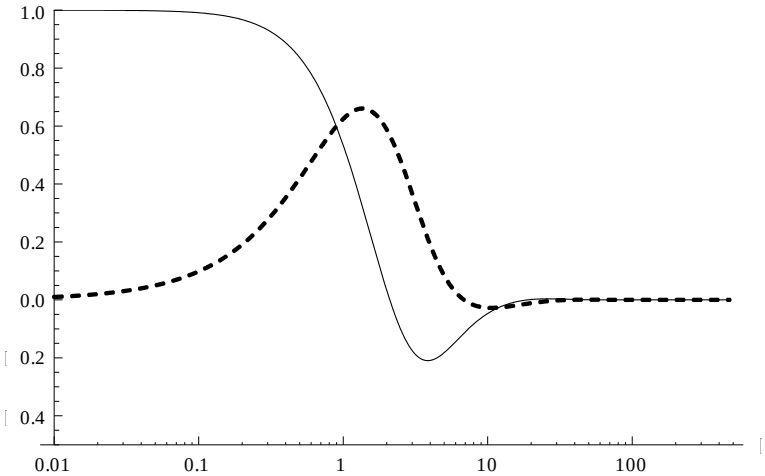

Figure 8 Complex Characteristic Function C(τ) versus τ for the Category II DH case
(real part=solid line, imaginary part=dashed line)

Note the FAF WP characteristic function approaches the form of the characteristic function $\exp(i\tau)$ associated with a unit step distribution, $U(z-1)$. Thus we would expect the FAF WP

distribution function to have a much steeper slope about the point $z = 1$ compared to the Category II distribution function.

4.3.2 Cumulative Probability Distribution Function Results

Table 4 below lists values of the cumulative distribution function 1-Pr(z) for the normalized aggregate received power density computed using equation (11) while figure 9 shows the same function as a graph for the three operational scenario cases.

Table 4 1-Pr(z) Values for each Operational Case

FAF WP		Cat. I DH		Cat. II DH	
z	**1-Pr(z)**	**z**	**1-Pr(z)**	**z**	**1-Pr(z)**
0.60	0.999999998	0.1000	0.99999985	0.1000	0.998145259
0.80	0.999983181	0.2000	0.9995299	0.2000	0.970721051
0.85	0.998333559	0.4000	0.95340299	0.4000	0.827553455
0.90	0.965915723	0.6000	0.78402089	0.6000	0.647897351
0.95	0.791716388	0.8000	0.56214627	0.8000	0.484818916
0.98	0.635102729	1.0000	0.37175546	1.0000	0.354978377
1.00	0.46239653	1.5000	0.1243844	1.5000	0.162058288
1.05	0.187674878	1.7500	0.07615466	1.7500	0.112429316
1.10	0.060554362	2.0000	0.04936027	2.0000	0.080134824
1.15	0.019026151	3.0000	0.01369834	3.0000	0.027025253
1.20	0.006859921	4.0000	0.00580826	4.0000	0.01246189
1.25	0.002995359	6.0000	0.00182011	6.0000	0.004277815
1.30	0.001539535	8.0000	0.00081124	8.0000	0.002020672
1.35	0.000889706	10.0000	0.00043367	10.0000	0.001129017
1.40	0.000558286	13.0000	0.00020611	13.0000	0.000566304
1.45	0.000371845	14.0000	0.00016705	14.0000	0.000464857
1.50	0.000259065	16.4722	0.00010414	16.4722	0.000301438
1.75	0.000064478	20.0000	5.9253E-05	20.0000	0.000178397
2.00	0.000023673	20.7635	5.3284E-05	20.7635	0.000160748
3.00	1.92E-06	30.0000	1.7550E-05	30.0000	0.000057775
4.00	4.08E-07				
6.00	5.20E-08				
8.00	1.20E-08				

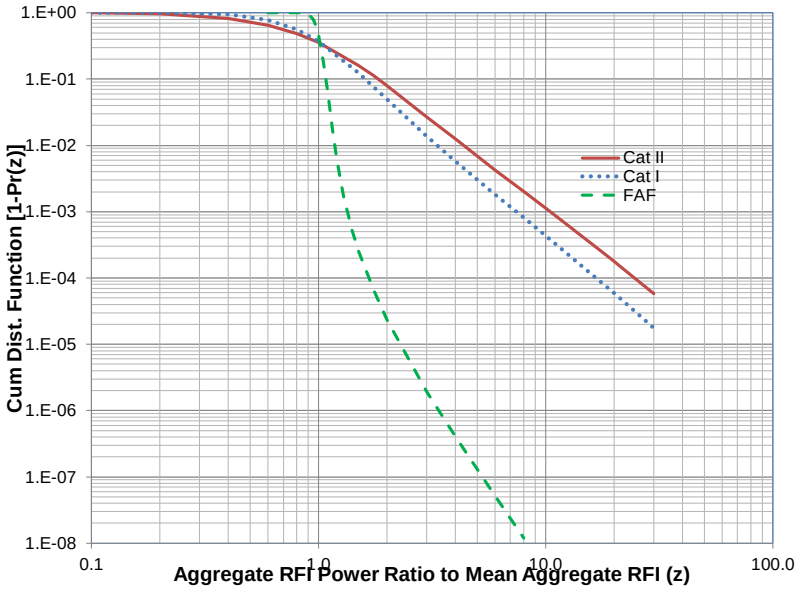

Figure 9 Cumulative Distribution Function, 1-Pr*(z)*, vs Normalized Power Density Ratio, *z*

As expected, the FAF WP case shows a steep slope around the point $z = 1$. Table 5 below shows the probability of the aggregate RFI power density exceeding the -140.5 dBW/MHz receiver MOPS test threshold and makes a comparison with results presented in [2].

Table 5 Probability of Aggregate Received RFI Density Exceeding MOPS Threshold

Case	Initial Model	Generalized Model
Cat II DH	8.996×10^{-3}	3.0144×10^{-4}
Cat I DH	4.275×10^{-3}	5.328×10^{-5}
FAF	3.1563×10^{-5}	$< 1.0 \times 10^{-8}$

The new generalized model shows a significant decrease (> 29x) in the threshold crossing probability compared to the results published in [2]. This is due largely to the small standard deviation associated with the log-normal fading component at short ranges (r < 100 meters) in the new model. The limited literature available describing probabilistic propagation for scenarios similar to those encountered in airport approaches with interferers located nearby [13], indicates that a range dependent standard deviation as used in the new model is more consistent with measured data.

While exceeding the MOPS RFI test threshold does not imply by itself that the GPS approach operation will be significantly impaired, the probabilities of threshold crossing for the Category I and II decision height cases are high enough, even with the generalized model, to cause some concern about operational continuity.

The cumulative distribution function, Pr*(z)*, has been computed to an accuracy of 9 decimal places. While this accuracy is deemed to be adequate, it does limit the ability to determine the probability of the aggregate RFI power density exceeding the MOPS test threshold. This accuracy limitation is evidenced in the FAF case where the threshold crossing occurs

for $z = \left(10^{-140.5/10} / \overline{P_I}\right) = 20.457$. From figure 9 it is clear that the threshold crossing probability is much less than 1×10^{-8} but the exact value is difficult to determine. It is possible to improve the accuracy beyond 9 decimal places, however at the expense of longer computation times.

5 Conclusion and Recommendations

A generalized analytic statistical model has been developed and presented for aggregate ground based RFI to airborne GPS receivers. The new model incorporates changes from previous models that more closely match propagation measurements presented in some of the recent literature. The model incorporates realistic path loss models accounting for the propagation environment likely to be encountered near large metropolitan airports. With the new model, numerical results have been obtained at 1575.42 MHz (GPS L1 center frequency) in three important cases for received aggregate mean interference power density, standard deviation, and the associated cumulative probability distribution function. With similar realistic estimates for emission power spectral density and surface concentration of emitters and other necessary parameters, the new generalized model results are reduced from those of the earlier model in [2]. However, they still indicate a cause for concern regarding the receiver MOPS RFI test threshold crossing probability for the Category I and II decision height cases. While recognizing that more information (such as the distribution associated with threshold crossing duration times) is needed to conclude that there will be substantial impairments to GPS measurements, none-the-less the greater than 16-fold reduction in threshold-crossing probability is an important result from the new model.

Because of the potential for RFI impact to operational continuity indicated above (table 5), an extensive RFI field test program may be needed to verify the new generalized analytic aggregate RFI model predictions. Such a test program was also recommended by RTCA SC-159 in conjunction with model refinement [1]. Before an extensive field test program is started, an intermediate step might involve inspecting flight test logs of GPS-equipped aircraft to extract the receiver's signal quality (C/N_0) measurements. These can be post-processed to determine an estimate of underlying RFI in different operational scenarios. If field tests are conducted, they would need to be done in the vicinity of several different airports and for various GPS antenna heights. Rather than using active test emitters as in cellular mobile telephone system propagation tests, passive power monitoring methods would have to be used to avoid generating RFI to other GPS users. Testing at the 1176.45 MHz GPS center frequency should also be considered.

Should these tests verify that the model parameter assumptions made in this report, including emission power spectral density and surface concentration of emitters, are realized in practice, then a further study is recommended into the probability distribution associated with threshold crossing duration times. Such a study would be needed to assess how significant are the predicted impairments to GPS-based flight operations that result from ground-based unwanted / unintentional interference.

References

[1] RTCA SC-159, “Assessment of Radio Frequency Interference Relevant to the GNSS L1 Frequency Band,” Doc. No. RTCA/DO-235B, RTCA, Inc., Washington, DC, March 13, 2008.

[2] K. M. Peterson and R. J. Erlandson, "Analytic Statistical Model for Aggregate Radio Frequency Interference to Airborne GPS Receivers from Ground-Based Emitters", Journal of the Institute of Navigation, Vol. 59, No. 1, Spring 2012.

[3] RTCA SC-159, “Assessment of the LightSquared Ancillary Terrestrial Component Radio Frequency Interference Impact to GNSS L1 Band Airborne Operations,” Doc. No. RTCA/DO-327, RTCA, Inc., Washington, DC, June 3, 2011.

[4] Status Report: Assessment of Compatibility of Planned LightSquared Ancillary Terrestrial Component Transmissions in the 1526-1536 MHz Band with Certified Aviation GPS Receivers, FAA Report PR 25, January 25, 2012.

[5] Hata, M., “Empirical formula for propagation loss in land mobile radio services,” *IEEE Trans. Veh. Technol.*, Vol. 29, pp. 317-325, Aug. 1980.

[6] Okumura Y., Ohmor E., Kawano T., and Fukua K., “Field strength and its variability in UHF and VHF land-mobile radio service,” *Rev. Elec. Commun. Lab.*, Vol. 16, No. 9, 1968.

[7] Erceg V., Greenstein L. J., Tjandra S. Y., Parkoff S. R., Gupta A., Kulic B., Julius A.A., and Bianchi R., “An Empirically Based Path Loss Model for Wireless Channels in Suburban Environments,” *IEEE Journal on Selected Areas in Communications*, Vol. 17, No. 7, July 1999.

[8] Parsons D., *The Mobile Radio Propagation Channel*. Chichester, England: John Wiley & Sons, 1996.

[9] Matthias Patzold, Ulrich Killat, and Frank Laue, "An Extended Suzuki Model for Land Mobile Satellite Channels and Its Statistical Properties", *IEEE Trans. on Veh. Technol.*, Vol. 47, No. 2, May 1998.

[10] Handout for graduate course on wireless comm. at the University of Illinois (ECE559) by professor V. V. Veeraldi: http://www.ifp.illinois.edu/~vvv/ece559/handouts/note3.pdf, pp. 53-56.

[11] John A. Gubner, "A New Formula for Lognormal Characteristic Function", *IEEE Trans. on Veh. Technol.*, Vol. 55, No. 5, Sept. 2006, pp. 1668- 1671.

[12] K.L. Chung, *A Course In Probability Theory*, Academic Press, New York, 1974.

[13] Loo, C., “A Statistical Model for a Land Mobile Satellite Link,” *IEEE Trans. on Veh. Technol.*, Vol. 34, No. 3, Aug. 1985.